



# Water Resources Research®



## METHOD

10.1029/2023WR035782

## A Unified Phenomenological Model Captures Water Equilibrium and Kinetic Processes in Soil

Yong Zhang<sup>1</sup> , Martinus Th. van Genuchten<sup>2,3</sup>, Dongbao Zhou<sup>4</sup>, Golden J. Zhang<sup>5</sup>, and HongGuang Sun<sup>6</sup> 

<sup>1</sup>Department of Geological Sciences, University of Alabama, Tuscaloosa, AL, USA, <sup>2</sup>Department of Nuclear Engineering, LASME, Federal University of Rio de Janeiro, UFRJ, Rio de Janeiro, Brazil, <sup>3</sup>Department of Earth Sciences, Utrecht University, Utrecht, The Netherlands, <sup>4</sup>School of Architecture and Civil Engineering, Anhui Polytechnic University, Wuhu, China, <sup>5</sup>College of Engineering, Texas A&M University, College Station, TX, USA, <sup>6</sup>The National Key Laboratory of Water Disaster Prevention, College of Mechanics and Materials, Hohai University, Nanjing, China

### Key Points:

- A tempered stable law with subordination built a unified model governing water equilibrium and kinetics in saturated/unsaturated soils
- Fractional-derivative equations fitted soil-water data sets, such as non-Darcian flow, as well as or better than classical models
- The assumed tempered stable density distribution for soil-hydraulic properties led to multi-rate moisture dynamics

### Supporting Information:

Supporting Information may be found in the online version of this article.

### Correspondence to:

Y. Zhang and H. Sun,  
yzhang264@ua.edu;  
shg@hhu.edu.cn

### Citation:

Zhang, Y., van Genuchten, M. Th., Zhou, D., Zhang, G. J., & Sun, H. (2024). A unified phenomenological model captures water equilibrium and kinetic processes in soil. *Water Resources Research*, 60, e2023WR035782. <https://doi.org/10.1029/2023WR035782>

Received 8 JULY 2023

Accepted 26 FEB 2024

### Author Contributions:

**Conceptualization:** Yong Zhang, Martinus Th. van Genuchten

**Data curation:** Yong Zhang,

Dongbao Zhou, Golden J. Zhang

**Formal analysis:** Yong Zhang,

Dongbao Zhou, Golden J. Zhang

**Funding acquisition:** Yong Zhang,

HongGuang Sun

**Investigation:** Yong Zhang, Golden J. Zhang

**Methodology:** Yong Zhang, Golden J. Zhang

**Project administration:** Yong Zhang,

HongGuang Sun

© 2024. The Authors.

This is an open access article under the

terms of the [Creative Commons](#)

[Attribution-NonCommercial-NoDerivs](#)

License, which permits use and

distribution in any medium, provided the

original work is properly cited, the use is

non-commercial and no modifications or

adaptations are made.

**Abstract** Soil water sustains life on Earth, and how to quantify water equilibrium and kinetics in soil remains a challenge for over a century despite significant efforts. For example, various models were proposed to interpret non-Darcian flow in saturated soils, but none of them can capture the full range of non-Darcian flow. To unify the different models into one overall framework and improve them if needed, this technical note proposes a theory based on the tempered stable density (TSD) assumption for the soil-hydraulic property distribution, recognizing that the underlying hydrologic processes all occur in the same, albeit very complex and not measurable at all the relevant scales, soil-water system. The TSD assumption forms a unified fractional-derivative equation (FDE) using subordination. Preliminary applications show that simplified FDEs, with proposed hydrological interpretations and TSD distributed properties, effectively capture core equilibrium and kinetic water processes, spanning non-Darcian flow, water retention, moisture movement, infiltration, and wetting/drying, in the soil-water system with various degrees and scales of system heterogeneity. Model comparisons and evaluations suggest that the TSD may serve as a unified density for the properties of a broad range of soil-water systems, driving multi-rate mass, momentum, and energy equilibrium/kinetic processes often oversimplified by classical models as single-rate processes.

**Plain Language Summary** This technical note introduced a framework aimed at unifying and enhancing existing theories/models for interpreting various soil-water processes in soils. A unified physical law, termed the “tempered stable density law,” was assumed for soil-water properties, leading to a unified model which well captures the core soil water processes that have been modeled (many times inefficiently) by tens of different and sometimes competing theories/models over the past century. This unified theory/model has the potential for expansion to other land-surface equilibrium and kinetic processes that cover a wide range of spatiotemporal scales and share a similar dynamic nature as water in soils.

## 1. Introduction

The soil-water system sustains terrestrial ecosystem functions (Knapp et al., 2008), and many physical laws and models have been proposed to quantify water equilibrium and kinetics for over a century. For example, various empirical and mechanistic models have been developed and are used routinely to describe moisture dynamics or equilibrium states in unsaturated soils, including unsaturated flow (Richards, 1931), soil water retention (Brooks & Corey, 1964; van Genuchten, 1980), and transient infiltration (Horton, 1933; Lewis, 1937). Some of these models, however, exhibit limitations in real-world applications (Sun et al., 2013). Modeling saturated flow, particularly non-Darcian flow, also remains challenging, as demonstrated below. This technical note aims to develop one theory/model to unify and, if necessary, improve these competing laws/models to interpret core soil-water processes, recognizing their occurrence in the same, although very complex, soil-water system.

The core assumption underlying this unified framework is that soil-water properties follow the tempered stable density (TSD) distribution. Unlike the standard stable density, which is a heavy-tailed (power-law) distribution with desirable mathematical properties (such as being applicable to all scales (called “infinitely divisible” in mathematics) (Samorodnitsky & Taqqu, 1994)), TSD truncates the standard stable density to allow a broader range of probability density functions (PDFs), including power-law, exponential, and various intermediate states.

**Resources:** Yong Zhang  
**Software:** Yong Zhang, Dongbao Zhou, Golden J. Zhang  
**Supervision:** Yong Zhang, HongGuang Sun  
**Validation:** Yong Zhang, Dongbao Zhou, Golden J. Zhang  
**Writing – original draft:** Yong Zhang, Golden J. Zhang  
**Writing – review & editing:** Martinus Th. van Genuchten, HongGuang Sun

This property makes TSD a common distribution for many hydrologic properties (Cvetkovic, 2011; Zhang et al., 2015).

In the following sections of this technical note, we (a) derive the unified model using the TSD assumption, (b) apply/validate the model by quantifying core equilibrium and kinetic processes for water in soil, and (c) identify TSD-distributed soil-water properties driving these diverse hydrologic processes. Instead of relying on tens of classical laws/models (many of which have limitations), this technical note introduces a unified model preliminarily validated for core hydrologic processes in the soil-water system. Furthermore, it has the potential for extension to other equilibrium/kinetic processes in the Earth system, as identified in Zhang, Sun, et al. (2017).

## 2. Methodology Development

We show that assuming a TSD distribution of soil-material properties, combined with the time subordination approach (explained below), leads to a unified fractional-derivative equation (FDE). Standard FDEs provide a promising tool to model non-Fickian transport of pollutants in heterogeneous aquifers (Zhang, Sun, et al., 2017) and other natural and social systems (Sun, Zhang, Baleanu, et al., 2018). The unified FDE extends the capabilities of standard FDEs by capturing stochastic processes in soil-water systems, as illustrated in this technical note.

Time subordination is a probability tool for converting physical time ( $t$ ) into operational time ( $\tau$ , which represents the period that the system is in its operating condition) for moving targets (Baeumer et al., 2001; Zhang, Baeumer, et al., 2017). Here, the operational time denotes the actual time that a water package would have spent in a dynamic state had it moved or transitioned at the mean rate, resulting in a random operational time for water packages driven by system heterogeneity. By adopting the TSD assumption, the governing equation for the resulting operational time density  $p$  in time-subordination takes the form (Zhang, Baeumer, et al., 2017):

$$\beta^* \frac{\partial p(t, \tau)}{\partial t} = \frac{\partial^{1-\gamma, \lambda}}{\partial t^{1-\gamma, \lambda}} \frac{\partial p(t, \tau)}{\partial \tau}, \quad (1)$$

where the subordinator corresponds to the TSD,  $\beta^* [T^{\gamma-1}]$  is a scale factor, and the symbol  $\partial^{1-\gamma, \lambda}/\partial t^{1-\gamma, \lambda}$  denotes the (exponentially tempered) Caputo fractional derivative defined by Meerschaert et al. (2008) with index  $1-\gamma$  [–] and truncation parameter  $\lambda [T^{-1}]$ . Combining Equation 1 with mass conservation, the time-subordinated water dynamics has a density function  $f$  that solves the following FDE (without source/sink terms):

$$\beta^* \frac{\partial f(x, t)}{\partial t} = [A] \frac{\partial^{1-\gamma, \lambda}}{\partial t^{1-\gamma, \lambda}} f(x, t), \quad (2)$$

where  $\beta^* = 1$  is used for unit conversion (no longer shown hereafter for description simplicity), and  $[A]$  is an operator (see examples shown in Table 1). Choosing  $\beta^* = 1$  is suitable for all applications in this study; however, its validity for other conditions/systems requires further confirmation. By rearranging the order of the fractional derivative in Equation 2, we obtain the equation governing the spatiotemporal evolution of  $f$ :

$$\frac{\partial^{\gamma, \lambda} f(x, t)}{\partial t^{\gamma, \lambda}} = [A] f(x, t), \quad (3)$$

where  $\Gamma(\cdot)$  is the gamma function.

The first term  $\partial^{\gamma, \lambda} f/\partial t^{\gamma, \lambda}$  in Equation 3 describes the memory impact on  $f$ : the status of  $f$  at the present time and location, denoted as  $f(x, t)$ , is affected by the historical condition  $f(x, \tau)$  (where  $0 < \tau \leq t$ ) at the same location whose weight declines as a TSD function in time (whose power-law exponent is  $\gamma$ ). This time-nonlocal memory impact exponentially declines for long historic times (when  $t - \tau \gg 1/\lambda$ ); therefore, the truncation parameter  $\lambda$  controls the maximum range of this memory impact. The second term  $[A]f(x, t)$  in Equation 3 describes the spatial dynamics of function  $f$  when  $[A]f(x, t)$  changes with  $f$  kinetically, or the rate of change of  $f$  when  $[A]f(x, t)$  defines an equilibrium constant.

In relatively homogeneous systems with local water dynamics uninfluenced by historical events or long-range neighbors, the index  $\gamma$  approaches 1 and Equation 3 simplifies to classical models featuring integer-order

**Table 1**  
Applications of the Unified FDE 4 to Ten Water-Related Processes in the Soil-Water System

Dynamics	Water-related processes	Function: $f$	Independent variable: $g$	Operator: $[A]$	TSD property	Standard laws/models: Limitation
Equilibrium	Non-Darcian flow: Equation 5	Darcy velocity	Pressure gradient	Hydraulic conductivity	Water retention & flow paths	Izbash's law, Forchheimer model, & Swartzendruber model: missing the full evolution of non-Darcian flow
	Water retention: Equation 12	Effective saturation	Pressure head	Rate	Soil pore size distribution	Brooks-Corey model: overestimating the pressure head near saturation (i.e., missing the SWRC transition)
	Adsorption isotherm (Zhou et al., 2021)	Solid-phase concentration	Aqueous-phase concentration	Rate	Multi-rate sorption/desorption	Langmuir model & Freundlich model: limited to monolayer or multi-layer, power-law rate adsorption (neglecting all the intermediate states)
Stable kinetics	Sediment suspension (Chen et al., 2013)	Sediment concentration	Water depth	Suspension index	Turbulent (bursting)	Rouse equation: missing the space nonlocal transport
	Turbulent flux (Sun, Zhang, Wei, et al., 2018)	Momentum	Vertical distance	Scaled shear velocity	Vertical velocity	Newton's law: fail to capture non-Newtonian dynamics
	Moisture movement: Equation 13	Water content	Time	(Net) Water flux	Statistics of water residence time and soil hydraulic conductivity	Richards equation: cannot capture non-Boltzmann scaling
	Water infiltration: Equation 15	Infiltration rate	Time	Maximum change of rate	Multi-rate decay due to soil texture and soil collides/air	Horton, Philip, and Lewis-Kostiakov models: missing the full evolution of infiltration rate
	Pollutant transport (Zhang, Sun, et al., 2017)	Chemical concentration	Time	Advection & dispersion	Multi-rate mass exchange	Fick's law: cannot capture non-Fickian diffusion of pollutants
	Heat flow in soil (Zhang et al., 2021)	Temperature	Time	Convection & conduction	Multi-rate thermal exchange	Fourier's law: missing non-Fourier heat transport
Non-stable Kinetics	Wetting/drying: Equation S12 in Supporting Information S1	Effective saturation	Time	Wetting and drying rates	Soil surface area & pore connectivity/size distribution	Not available

*Note.* The parameters  $f$ ,  $g$ , and  $[A]$  denote the function, independent variable, and operator in Equation 4, respectively. Additionally, sediment, pollutant, turbulent, and thermal equilibrium or transport processes are included to illustrate the extension of FDE 4 for quantifying mass, momentum, and energy transport in geologic media, including the soil-water system. The last column lists the classical law/model(s) for each water-related process along with their intrinsic limitations, which can be addressed by FDE 4.

derivatives like Darcy's law or Richards' equation, as discussed below. For fractional derivatives with  $\gamma \in (0, 1)$ , a smaller  $\gamma$  can capture a stronger nonlocal impact, particularly in more heterogeneous soil-water systems (deviating further from the local case with  $\gamma = 1$ ). This can be observed in saturated high-permeability media where random flow paths induce a pronounced spatially nonlocal impact on non-Darcian flow (refer to Text S1.2 in Supporting Information S1), and in unsaturated soils with a wider pore size distribution where the soil water retention curve (SWRC) slope undergoes a more gradual change in the capillary regime (refer to Section 3.2). When  $\gamma \in (1, 2)$ , a larger  $\gamma$  (deviating further from the case of  $\gamma = 1$ ) can capture a stronger nonlocal impact (especially in time), exemplified in Application #1 (Section 3.1) for low-velocity non-Darcian flow, where a TSD memory function is linked to water retention in low-permeability media.

By adopting the variable index defined by Sun et al. (2019) and generalizing the independent variable, we obtain the unified FDE:

$$\frac{\partial^{\gamma(g), \lambda(g)} f(g)}{\partial g^{\gamma(g), \lambda(g)}} = [A]f(g), \quad (4)$$

where  $g$  denotes the independent variable (with  $f$  becoming a function of  $g$ ). After defining  $f$ ,  $g$ , and  $[A]$ , Equation 4 can model core water equilibrium/kinetic processes in soils described below.

### 3. Method Applications

#### 3.1. Application #1: Equilibrium Non-Darcian Flow in Saturated Soil

Non-Darcian flows, characterized by the non-linear growth of fluid velocity with respect to the increasing pressure gradient in saturated media, are well-documented in fluid flow with small velocities in unconsolidated sand or sedimentary rocks (Nimmo, 2021; Soni et al., 1978) and high velocities in fractured media (Şen, 1987). Tremendous efforts have been dedicated to quantifying non-Darcian flow for over a century, resulting in well-known models, including Izbash's law (Izbash, 1935), the Forchheimer model (Forchheimer, 1901), and the Swartzendruber model (Swartzendruber, 1962). To unify and enhance these models, we simplify the unified FDE 4 as the Equilibrium-FDE 5:

$$\frac{\partial^{\gamma, \lambda} q}{\partial J^{\gamma, \lambda}} = K, \quad (5)$$

where  $q$  [L/T] is the fluid velocity,  $J$  [-] is the absolute value of the hydraulic gradient, and  $K$  [L/T] is the effective hydraulic conductivity. Equation 5 can also be derived using structure derivatives, as shown in Text S1.1 in Supporting Information S1. The analytical solution of Equation 5 is:

$$q = K E_{1, \gamma+1}^{\gamma}(-\lambda J) J^{\gamma}, \quad (6)$$

where  $E_{1, \gamma+1}^{\gamma}(\cdot)$  denotes the generalized Mittag-Leffler function:  $E_{\eta, \mu}^{\gamma}(z) = \sum_{k=0}^{\infty} \frac{\Gamma(\gamma+k)/\Gamma(\gamma)}{\Gamma(\eta k + \mu)} \frac{z^k}{k!}$ . We note that Mainardi (2020) defined the Mittag-Leffler function as the “queen function” of fractional calculus since it continuously interpolates between purely exponential law and power-law-like functions; those properties are highly relevant to our study. FDE 5 can also be applied to other equilibrium pairs in hydrology and geo-engineering, such as the asymptotic vertical distribution of suspended sediment in rivers/streams (Chen et al., 2013) and the creep of frozen soil (Gu et al., 2023). Its applications in other equilibrium states, including total or component mass balance, summation, and energy balance (Cantele et al., 2021; Rodriguez-Robles et al., 2019), remain to be explored.

Equation 5 uses the truncation parameter  $\lambda$  to regulate the transition from non-Darcian flow to Darcian or other non-Darcian flows. Such a broad transition was overlooked by existing non-Darcian models. For example, when  $\lambda = 0$  (neglecting state transition), Equation 5 reduces to  $\partial^{\gamma} q / \partial J^{\gamma} = K$ , and its solution, Equation 6, reduces to the empirical Izbash's law (Benedikt et al., 2018):

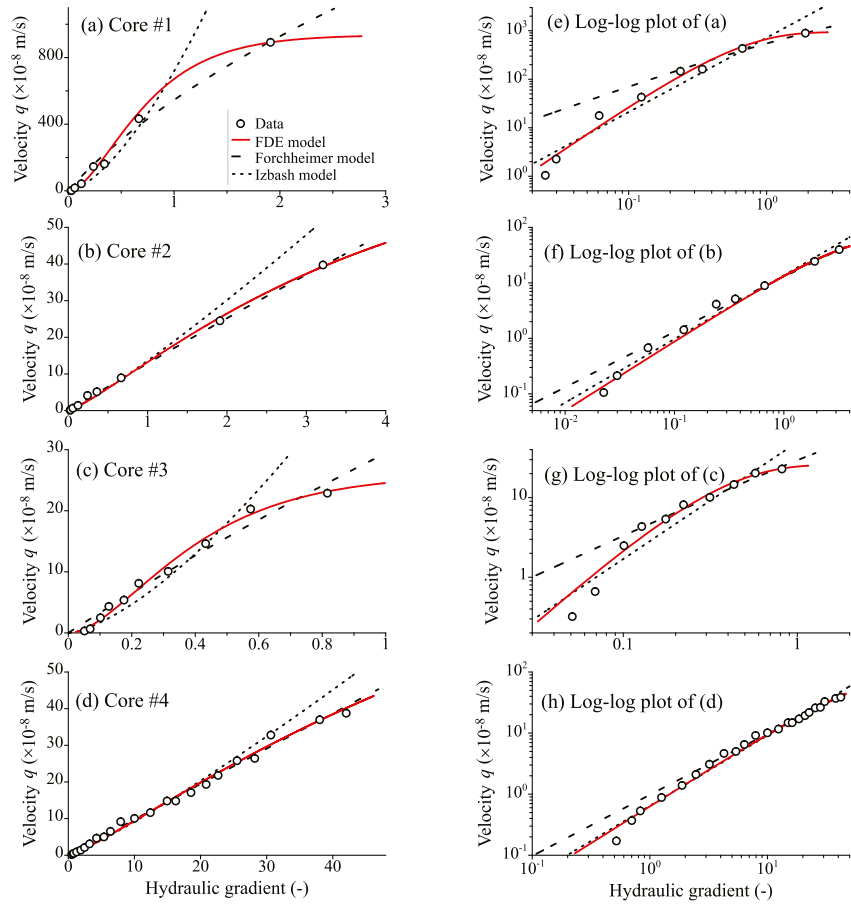


**Figure 1.** Application #1: Non-Darcian flow of an organic fluid (Soltröl-130) through sandstone in Core 1 (a), Core 2 (b), Core 3 (c), and Core 4 (d), respectively. The symbols denote measurements by Siddiqui et al. (2016), and the lines represent the best-fit solutions using different models, with the best-fit parameters listed in Table S1 in Supporting Information S1.

$$q = KJ^\beta. \quad (7)$$

Izbash's law 7 captures low-velocity non-Darcian flow but is unable to model the transition between Darcian and non-Darcian flows, or that between various non-Darcian flows. To incorporate both Darcian and non-Darcian flows, the Forchheimer model (derived from the Navier-Stokes equation or the capillary tube approach) takes the form (Takhanov, 2011):

$$J = \frac{\mu}{k} q + \eta \rho q^2, \quad (8)$$

where  $\mu$  [Pa·T] is the fluid dynamic viscosity,  $k$  [L<sup>2</sup>] is the medium permeability,  $\eta$  [L<sup>-1</sup>] is the inertial resistance, and  $\rho$  [M·L<sup>-3</sup>] is the fluid density. On the right-hand side (RHS) of the Forchheimer model 8, the 1st term captures Darcian flow affected by viscous force at low velocities, and the 2nd term describes quadratic flow due to inertial resistance at large pressure drops and high velocities (such as flow in the vicinity of a pumping well). Hence, Equation 8 reduces to Darcy's law at low velocities, missing (a) low-velocity non-Darcian flow where the  $q(J)$  curve has an initial power-law slope steeper than 1, and (b) flow in low-permeability media where the  $q(J)$  curve is concave up in a linear-linear plot, requiring a negative  $\beta$  in Equation 8. To efficiently capture widely observed low-velocity non-Darcian flow, the Swartzendruber model takes the form (Swartzendruber, 1962):

$$q = K \left[ J - J^* \left( 1 - e^{-J/J^*} \right) \right], \quad (9)$$

where  $J^*$  represents the threshold hydraulic gradient. In Equation 9, the change of fluid velocity with respect to the pressure gradient increases exponentially (whose rate is controlled by the threshold  $J^*$ ) before approaching its asymptote  $K$  at  $J \gg J^*$  (i.e., transition to Darcian flow). Therefore, the Swartzendruber model 9 misses high-velocity non-Darcian flow.

These models are checked against real-world data, with one representative result plotted in Figure 1. Additional details and other cases are presented in Text S1.2 in Supporting Information S1. These applications support the analysis mentioned above: Izbash's law 7 fails to capture the velocity-dependent slope of the observed  $q(J)$  curves, the Forchheimer model 8 misses low-velocity non-Darcian flow, the Swartzendruber model 9 overlooks high-velocity non-Darcian flow, and the FDE 5 emerges as the only viable option capable of capturing the full-range of non-Darcian flow.

Non-Darcian flow has two main triggers. Trigger #1 involves microscopic inertial effects (Forchheimer, 1901; Ruth & Ma, 1992) and increasing microscopic viscous force (Hassanizadeh & Gray, 1987), generating non-Darcian flow at high velocities. Trigger #2 includes heterogeneities in sample permeability or flow velocity, flow streamlining, and pore participation number (Barree & Conway, 2005), non-Newtonian flow (Kutiřek, 1972), or boundary layer effects (Wang et al., 2018), causing low-velocity non-Darcian flow. Here, we interpret non-Darcian flow using the FDE 5. For low-permeability materials with usually low flow rates, the best-fit index  $\gamma$  in FDE 5 is between 1 and 2 (Text S1.2 in Supporting Information S1), where the fractional derivative can be expanded as:

$$\frac{d^{r,\lambda}}{dJ^{r,\lambda}}q = \frac{d^2q}{dJ^2} * g(J) = \frac{1}{\Gamma(2-\gamma)} \int_J^\infty \frac{d^2q}{d\tau^2} e^{-\lambda\tau} \nu(J-\tau)^{1-\gamma} d\tau, \quad (10)$$

where the symbol “\*” denotes convolution, and  $g(J) = \frac{1}{\Gamma(2-\gamma)} \int_J^\infty e^{-\lambda\tau} \gamma \tau^{1-\gamma} d\tau$  is the TSD memory function. Equation 10 can be approximated using the one-shift Grünwald formula for  $\lambda \rightarrow 0$  (Meerschaert & Tadjeran, 2004):

$$\frac{d^{r,\lambda}}{dJ^{r,\lambda}}q \approx \frac{1}{(\Delta J)^\gamma} \sum_{i=0}^N f_i q[J - (i-1)\Delta J] = \frac{1}{(\Delta J)^\gamma} \left\{ q(J + \Delta J) - \gamma q(J) + \sum_{i=2}^N f_i q[J - (i-1)\Delta J] \right\} \quad (11)$$

where  $\Delta J$  is the step size discretizing the pressure gradient,  $N$  is a sufficiently large number of grid points of the pressure gradient, and  $f_i = \frac{\Gamma(i-\gamma)}{\Gamma(-\gamma)\Gamma(i+1)}$  is the Grünwald weight (the summation of these weights equals 1 for  $i = 0, 1, 2, \dots$ , and  $f_i > 0$  for  $i \geq 2$  when  $1 < \gamma < 2$ ) whose absolute value decreases with an increasing sequence  $i$ .

Equation 10 implies that the change of  $q$  with  $J$  is a nonlocal process. Water moving in low-permeability soil can be retarded by fluid-rock interactions (Oelkers & Schott, 2018), sorption-desorption at the mineral/water interface (Scheidegger & Sparks, 1996), and mass exchange between the main flow zone and the surrounding less-mobile regions or between soil/aquifer zones (Eberts & George, 2000). These less mobile water packages can be reactivated with a remobilization probability proportional to the Grünwald weight  $|f_i|$  as shown in Equation 11. This nonlocal impact is described by the summation of all the “less-mobile water” terms marked by the sequence  $i \geq 2$  (all the terms except  $-\gamma q(J)$  on the RHS of Equation 11 are positive, because  $f_i > 0$  for  $i > 2$ ), explaining the positive concavity of the  $q(J)$  curve in a linear-linear plot, as shown, for example, in Figure S1 in Supporting Information S1.

In the FDE 5, the index  $\gamma$  defines the overall degree of the nonlocal impact, where a larger  $\gamma$  captures a stronger nonlocal impact (represented by a relatively larger positive concavity) and a larger power-law slope (deviating more from linear flow) of the  $q(J)$  curve (e.g., Table S2 and Figure S1 in Supporting Information S1). In addition, the truncation parameter  $\lambda$  controls the transition from pre-Darcian to Darcian flow: low-velocity non-Darcian flow occurs for the hydraulic gradient  $J \ll 1/\lambda$ , gradually shifting to Darcian flow with increasing  $J \gg 1/\lambda$ . For the special case of  $\gamma = 1$ , all the “historical” components in Equation 11 disappear (i.e., without the “nonlocal” impact), and Equation 11 reduces to the forward first-order difference which defines Darcy flow, as expected. Therefore, an FDE 5 with an index  $\gamma$  between 1 and 2 characterizes low-velocity non-Darcian flow, likely due to the nonlocal impact with a TSD memory function related to water retention in low-permeability media. Similarly, high-velocity non-Darcian flow may be due to the spatially nonlocal impact related to random flow paths with a

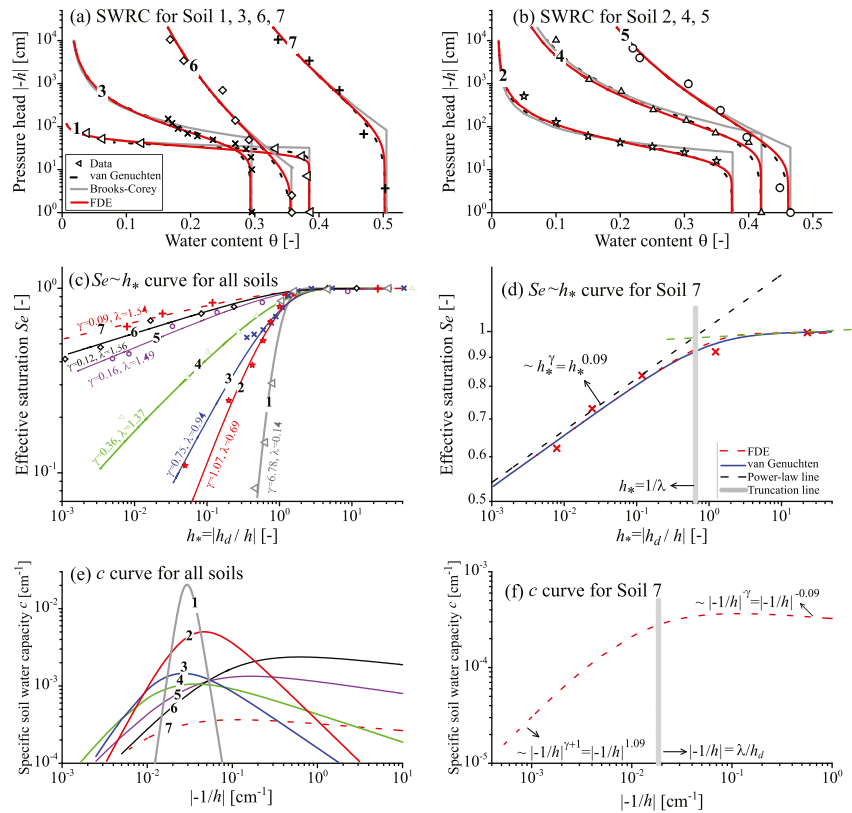


**Figure 2.** Application #2: Measured (symbols, from Novák and Hlaváčiková (2019)) versus best-fit model results for the SWRC of Soils 1 through 7 in (a) and (b). The optimized parameters are listed in (c). The  $S_e(h_*)$  curve for all 7 soils (c), with Soil 7 plotted again in (d) to show the power-law slope. Plot (e) shows the specific soil water capacity curve for these 7 soils, with Soil 7 plotted again in (f) to show the power-law slope.

TSD distribution in high-permeability media, and it can be captured by Equation 5 with a  $\gamma$  between 0 and 1 (see Text S1.3 in Supporting Information S1). Therefore, the TSD memory function due to soil-water heterogeneity may drive both low- and high-velocity non-Darcian flows and the subsequent transition, expanding on trigger #2 mentioned above for non-Darcian flow.

### 3.2. Application #2: Equilibrium Water Retention in Unsaturated Soil

The unified FDE 4 also links water content  $\theta$  and pressure head  $h$  in unsaturated soil:

$$\frac{\partial^{\gamma, \lambda}}{\partial (h_*)^{\gamma, \lambda}} S_e = k, \quad (12)$$

where  $S_e = (\theta - \theta_r) / (\theta_s - \theta_r)$  [–] is the effective saturation;  $\theta$ ,  $\theta_r$ , and  $\theta_s$  [–] are the volumetric, residual, and saturated water contents, respectively;  $h_* = |h_d|/|h|$  [–], with  $h_d$  [L] representing the air entry value; and the rate  $k$  [–] can be approximated by  $k \approx [|h_d|^\gamma E_{1, \gamma+1}^\gamma(-\lambda |h_d|)]^{-1}$ , or simply calculated by  $k = \Gamma(\gamma + 1)$  if the index  $0 < \gamma < 1$  or  $\lambda$  is small (e.g.,  $\lambda < 1$ ). The Equilibrium-FDE 12 (the same form as Equation 5) models a temporally nonlocal change of water content with the pressure head in multiple rates whose distribution follows the TSD. This results in an upper-truncated power-law decline of  $S_e$  at large  $h_*$ , with the corresponding soil water retention curve (SWRC) exhibiting the shape of a sigmoid curve at small  $|h|$ .

One application is depicted in Figures 2a and 2b. Novák and Hlaváčiková (2019) collected the SWRC drainage branches of typical soils, including nearly monodispersed glass sand (Soil 1), a sandy soil (Soil 3), and a fine-textured (clay) soil (Soil 7). The index  $\gamma$  is approximated by the log-log slope of the initial rising limb of the observed  $S_e(h_*)$  curve (Figure 2c), consistent with Equation 12. This power-law portion of the  $S_e(h_*)$  curve covers

the capillary and adsorption regions, which involve water flow in small pores. The truncation parameter  $\lambda$ , which captures the upper bound of the heavy-tailed power-law function  $S_e(h_*)$ , can be approximated by the cross point of the two power-law sections of  $S_e(h_*)$  (Figure 2d). Model comparisons in Text S2.1 in Supporting Information S1 show that FDE 12 is closely related to the van Genuchten model, the most reliable model for fitting various SWRCs (the two models provide almost identical fits), and it improves the Brooks-Corey model by capturing the transition of the SWRC slope (Figures 2a and 2b). The close fit observed between FDE 12 and the van Genuchten model can be attributed to the algebraic relationship of parameters shared between these two models, as illustrated in Text S2.1 in Supporting Information S1. This connection suggests that the FDE may provide a potential method for associating these model parameters with soil-water properties.

The physical meanings of model parameters  $\gamma$  and  $\lambda$  can be interpreted using the concept of capillary tubes. Equation 12 assumes the TSD distribution of the soil pore size  $r$  (usually within the range of 50–0.5 mm), denoted as  $f(r)$  here. According to cylindrical capillary bundle models (e.g., Millington & Quirk, 1961; Novák & Hlaváčiková, 2019), all capillary tubes of radius  $r > R_j$  are drained at a given  $h_j$  (following the capillarity equation  $R_j \propto -1/h_j$ ). Since large pores are known to fill or empty at small pressure heads ( $|h| \rightarrow 0$ ), a PDF  $f(r)$  with many large pores results in the SWRC dropping quickly at small values of  $|h|$ . The section of  $f(r)$  for fine pores, on the other hand, controls the SWRC slope, with a wider pore size distribution leading to a more gradual change in the SWRC slope mainly in the capillary regime (Nimmo, 2004), which can be captured by a smaller index  $\gamma$  in Equation 12 (see Figure 2c). While the above-mentioned description ignores the effects of film, corner, and vapor flow in the very dry range (e.g., Iden et al., 2021), the macroscopic form is realistic for many soils. Therefore, the PDF  $f(r)$  for fine pores defines the range of  $\gamma$ , and the transition from fine to large pores in  $f(r)$  defines the value of  $\lambda$ .

We further correlate the soil pore size distribution and the FDE index  $\gamma$ . The specific soil water capacity,  $c = d\theta/dh$  of a drying  $\theta(h)$  curve, approximates the PDF of the combined volume of all pores whose effective radius is centered at  $r$  (Figure 2e). For example, Soil 1 (glass sand) had a narrow  $f(r)$  (Novák & Hlaváčiková, 2019) (see the line “1” in Figure 2e), resulting in a relatively flat SWRC (like a step function shown by curve “1” in Figure 2a) which can be captured by Equation 12 with the largest index  $\gamma$  and the smallest truncation parameter  $\lambda$  of the seven soils (listed in Figure 2c). Soil 7 (clay), on the other hand, had a relatively broad  $f(r)$  (Figure 2e), whose much steeper SWRC (see Figure 2a) can be captured by Equation 12 using small  $\gamma$  and large  $\lambda$  values. Additional analyses in Text S2.2 in Supporting Information S1 also show that the power-law slope of the pore volume distribution is linearly related to the FDE index  $\gamma$ .

### 3.3. Application #3: Soil Moisture Movement Kinetics

Unsaturated flow can exhibit strong variations in both space and time, involving more soil-water properties than equilibrium water retention. When  $f = \theta$ ,  $g = t$ , and  $[A]$  denotes the differential Buckingham-Darcy flux, the unified FDE 4 reduces to the Flow-FDE 13, quantifying unsaturated flow:

$$e^{-\lambda t} \frac{\partial^\gamma (e^{\lambda t} \theta)}{\partial t^\gamma} = \frac{\partial}{\partial x_i} \left[ D_w(\theta) \frac{\partial \theta}{\partial x_i} \right] + \frac{\partial}{\partial x_i} \left[ K(\theta) \frac{\partial z}{\partial x_i} \right], \quad (13)$$

where  $x_i$  [L] denotes the direction of water movement,  $D_w(\theta) = K(\theta)dh/d\theta$  [ $L^2/T$ ] is the soil water diffusivity, and  $K(\theta)$  [ $L/T$ ] is the unsaturated soil hydraulic conductivity. When  $\lambda \rightarrow 0$ , the Flow-FDE 13 reduces to the standard time-fractional Richards equation as shown by Gerolymatou et al. (2006). When  $\gamma = 1$  and  $\lambda \rightarrow 0$ , the Flow-FDE 13 further reduces to the classical Richards equation (Richards, 1931):

$$\frac{\partial \theta}{\partial t} = \frac{\partial}{\partial x_i} \left[ D_w(\theta) \frac{\partial \theta}{\partial x_i} \right] + \frac{\partial}{\partial x_i} \left[ K(\theta) \frac{\partial z}{\partial x_i} \right]. \quad (14)$$

Hydrological interpretation of the Flow-FDE 13 may be related to the multi-rate, or so-called “anomalous,” water transport in unsaturated media proposed by several authors (Gerolymatou et al., 2006; Sun et al., 2013). Water moves in soil with both fast flow (via local preferential pathways such as structural voids or biological channels) and slow components (e.g., moving along sinuous paths, trapped by relatively low-permeability or immobile zones, or delayed by mass exchange between mobile and stagnant regions), generating a random operational time



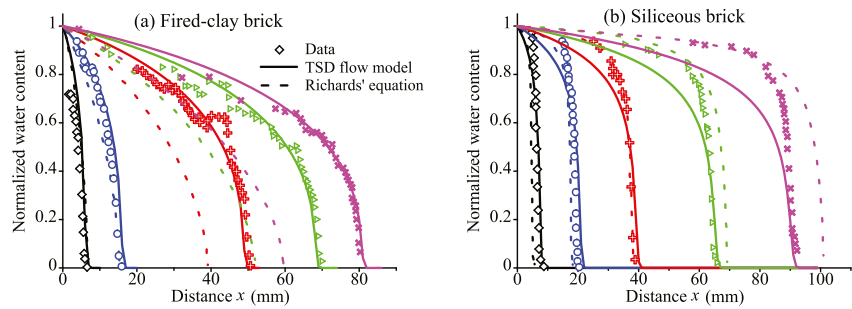


**Figure 3.** Application #3: Non-Boltzmann scaling of wetting fronts (horizontal infiltration). (a) Experimental wetting front data (El-Abd & Milczarek, 2004) in a fired-clay brick, with fitted modeling results using a power-law diffusivity. Corresponding times for the five sets of data are  $t = 419, 2219, 14879, 26099,$  and  $34559$  s. The optimized diffusivity function for the Richards Equation 14 was  $D_w(\theta) = 7.5 \times 10^{-2} \theta^{1.75}$ . For the Flow-FDE 13, the best-fit data were  $D_w(\theta) = 1.9 \times 10^{-2} \theta^{2.25} \text{ mm}^2 \text{ s}^{-\gamma}$ ,  $\gamma/2 = 0.60$  ( $\gamma/2 > 0.5$  in the FDE for super-diffusion), and  $\lambda_r = 0$ . (b) Experimental data and model fits for a siliceous brick. The times for the five distributions are  $t = 450, 5370, 24210, 79770,$  and  $170430$  s. The solution curves for Flow-FDE were obtained using an exponential diffusivity  $D_w(\theta) = 1.78 \times 10^{-4} \exp(8.4\theta) \text{ mm}^2 \text{ s}^{-\gamma}$  with best-fit  $\gamma/2 = 0.43$  ( $\gamma/2 < 0.5$  for sub-diffusion) and  $\lambda_r = 1.0 \times 10^{-5} \text{ s}^{-1}$ . The water content curves for the Richards equation were reproduced from Figure 9 in Gerolymatou et al. (2006).

(distributed as TSD) for water packages and therefore “anomalous” dynamics. For example, when  $\lambda = 0$  and  $D_w$  is constant in the FDE 13, the spatial variance of horizontal moisture movement increases nonlinearly in time (Zhang et al., 2008):  $\sigma^2(t) = 2D_w t^\gamma / \Gamma(\gamma + 1)$ , which captures super-diffusion with  $\gamma/2 > 0.5$  and sub-diffusion with  $\gamma/2 < 0.5$ .

Two applications for horizontal water flow are shown in Figure 3. In such instances, solving the nonlinear Flow-FDE 13 requires the use of a numerical solver (developed in Text S5 in Supporting Information S1). Results showed that the classical Richards Equation 14 either underestimated the super-diffusive water content front (Figure 3a) or overestimated the sub-diffusive water content front (Figure 3b). This is because Equation 14 assumes that the horizontal travel distance of moisture grows as the square root of time (i.e., Boltzmann scaling), while real-world horizontal flow often exhibits non-Boltzmann or “anomalous” scaling (e.g., Sun et al., 2013) described by the Flow-FDE 13. Notably, the non-Boltzmann scaling can also be effectively quantified through the fractal Richards equation, as demonstrated by Sun et al. (2013). A concise comparison between the fractional and fractal Richards equations is provided in Text S5 in Supporting Information S1. Additionally, the fractional Richards Equation 13 can be linearized using the TSL and full subordination, as detailed in Text S6 in Supporting Information S1.

Saturated flow dynamics, the core process in hydrogeology studies, may have similar mechanisms. For example, transient flow in confined aquifers is “anomalous” and can be captured by a simplified Flow-FDE 13 by assuming  $\lambda = 0$  and replacing the water content with the hydraulic head in Equation 13 (Xia et al., 2021).

### 3.4. Application #4: Water Infiltration Kinetics

The water infiltration rate  $i(t)$ , especially during ponding, into a soil usually declines with a variable deceleration rate in time (Jury & Horton, 2004). It is well-known that the infiltration rate is high at the beginning of a storm or ponded irrigation (denoted as  $i_0$  [L/T]) when the soil is dry, and then decreases as the soil becomes saturated, ultimately approaching an asymptote value  $i_f$  at or close to the profile-averaged saturated hydraulic conductivity. Many empirical models exist for describing water infiltration into soils, including the widely applied Horton, Green-Ampt, and Philip equations (Philip, 1957; Rahmati et al., 2022). To unify and improve these models, we simplify the unified FDE 4 to the Kinetic-FDE 15:

$$\frac{\partial^{\gamma, \lambda}}{\partial t^{\gamma, \lambda}} f = (i_0 - i_f) f, \quad (15)$$

with  $f = i_0 - i(t)$ ,  $g = t$ , and  $[A]$  denoting the fluctuation of the infiltration rate  $i_0 - i_f$ . The solution is:

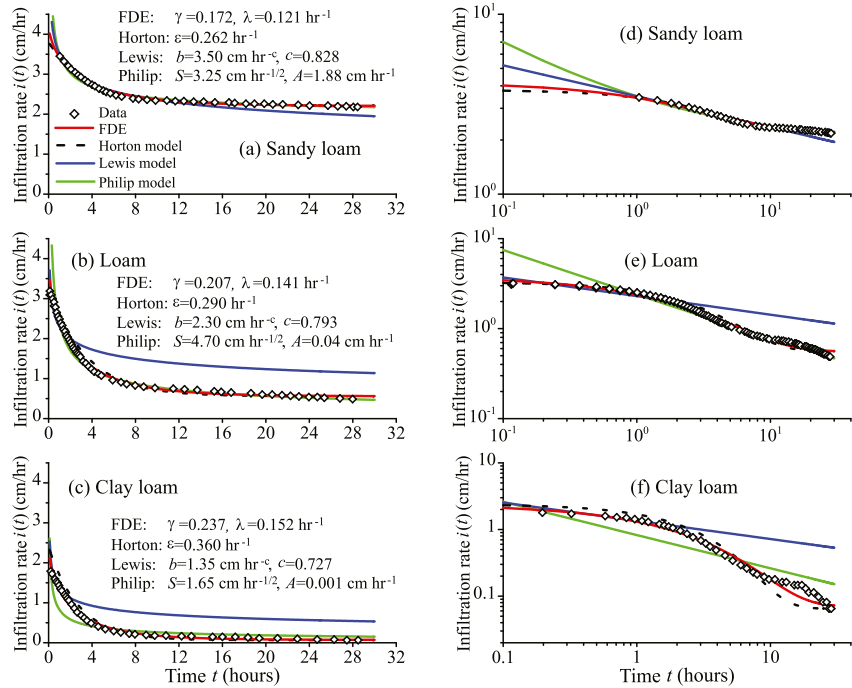


**Figure 4.** Application #4: Change in infiltration rate with time. Measured data (symbols) versus the model fit (lines) for sandy loam (a), loam (b), and clay loam (c). The right plot is a log-log version of the left plot, emphasizing early- and late-time tailing behavior.

$$i(t) = i_0 - (i_0 - i_f) [t^{1-\alpha} E_{1,2-\alpha}^{-\alpha}(-\lambda t) - \lambda^\alpha t]. \quad (16)$$

The Kinetic-FDE solution 16 captures various evolutions of the infiltration rate, including a power-law function, an exponential function, and a constant asymptote. Equation 16 for this purpose contains the Horton and Philip equations as end members. For example, when  $\lambda = 0$ , Equation 16 reduces to the power-law form  $i(t) \propto t^{1-\alpha}$ , which is analogous to the Lewis-Kostiakov model (Lewis, 1937):

$$i(t) = b t^{c-1}, \quad (17)$$

where  $b$  and  $c$  are empirical constants depending on soil type, and the Philip model for vertical infiltration:

$$i(t) = \frac{S}{2\sqrt{t}} + A, \quad (18)$$

over a relatively short time (where  $S$  and  $A$  are constants). When  $\lambda$  is large, the Kinetic-FDE solution 16 reduces to a single infiltration rate model analogous to the exponential Horton model 19:

$$i(t) = i_f + (i_0 - i_f) e^{-\epsilon t}, \quad (19)$$

where  $\epsilon$  [ $\text{hr}^{-1}$ ] is an empirical parameter describing the rate of decrease of infiltration.

We tested these models by fitting real-world data (Figure 4). Results revealed that the Kinetic-FDE solution 16 captures the observed transient infiltration rate slightly better than the other models, with the Lewis model 17 and Horton model 19 producing correct solutions only for early times ( $t \ll 1/\lambda$ ) and late times ( $t \gg 1/\lambda$ ), respectively. This is because the solution 16 describes an exponentially truncated power-law function using the power-law portion for times  $t \ll 1/\lambda$  and the exponential portion for times  $t \gg 1/\lambda$  (we recall here that the Mittag-Leffler function can be used to interpolate continuously between Gaussian and Lorentzian functions). By comparison,

the Lewis and Horton models are based on a power-law function and an exponential function, respectively, for the transient infiltration rate process. In addition, the Philip model 18 assumes a constant power-law exponent (0.5) for the full evolution of the infiltration rate for all soils, which is clearly not consistent with all the data.

## 4. Discussion and Conclusion

### 4.1. TSD of Soil-Hydraulic Properties

The TSD assumption underlying the FDE 4 is analogous to the fractal morphology assumed in fractal models for soil structure. Various models have been proposed to relate the empirical SWRC fitting parameters to the fractal dimension of soil pore or particle size distributions (e.g., Pachepsky et al., 1995; Zhao, 2020). Soil pores display self-similar scaling with an infinite nesting structure of micropores, macropores, and mesopores. The internal structure, pore size distribution, and pore geometry of soil exhibit fractal features, which can be characterized by different fractal dimensions (Giménez et al., 1997). Independent studies have also demonstrated a close relationship between the fractal dimension and the FDE index (Verma & Viswanathan, 2020). The FDE 4 offers greater flexibility than standard fractal models in applications, since it allows (a) a single fractional index to encompass multiple fractal dimensions or intrinsic dimensions of soil (Giménez et al., 1997), and (b) captures the impact of hydraulic properties on water processes. In addition, the truncation parameter  $\lambda$  defines the upper or, in some cases, lower limit of the power-law distribution of soil and hydraulic properties listed in Table 1. This truncation is necessary as natural processes are generally bounded, distinguishing TSD from the standard stable density.

Significantly, it is essential to recognize that the TSD-based FDE 4 is not designed as a predictive model, constituting the principal limitation of this note. Further discussion on this limitation is provided in Text S4 in Supporting Information S1. Detailed information on the soil-water properties driving water equilibrium/kinetics (referencing column 6 in Table 1) was not provided by most applications discussed above (explained in Text S2.2 in Supporting Information S1). Further experimental efforts, hence, are needed to detect the distribution of the soil-water properties identified theoretically in this note to improve the FDE's predictability. This technical note focuses on water flow rather than chemical reactions. Chemical reactions in heterogeneous media may involve properties beyond those related to soil and water. Extending the analysis to include chemical reactions can be challenging (Bolster et al., 2017) and may necessitate reformulation, particularly in the presence of structural heterogeneity causing non-uniform reactivity across exchange rates (Painter, 2021; Roche & Dentz, 2022) or in cases where reactions are mixing-limited (Dentz et al., 2011). Notably, the TSD theory may potentially be expanded to integrate chemical reactions as an additional term in FDE 4. For instance, the time-dependent chemical reaction rate, influenced by incomplete mixing of reactants in heterogeneous porous media, may exhibit a power-law decline (before reaching its asymptote) (Sanchez-Vila et al., 2010). This could lead to a fractional-order advection-dispersion-reaction equation, as proposed by Zhang (2023). We will explore this topic in future research.

### 4.2. Model Generalization and Application in Earth Sciences

If a source-sink term is present (and denoted as  $r$ ), the FDE 4 can be expressed as:

$$\frac{\partial^{\gamma(g),\lambda(g)} f(g)}{\partial g^{\gamma(g),\lambda(g)}} = [A]f(g) + e^{-\lambda(g)g} \int_g^\infty e^{\lambda(s)s} r(x,s) \frac{\gamma(s)s^{-\gamma(s)-1}}{\Gamma(1-\gamma(s))} ds, \quad (20)$$

where the last term captures the time-nonlocal source/sink term (in contrast to the classical, time-local source/sink term). It is important to note that this source-sink term has not been considered in the applications shown above, and its relevance and formulation necessitate further exploration.

Water flow in soils can be conceptualized as a multi-rate mass transfer (MRMT) process occurring between connected pores (containing mobile water) and relatively immobile regions (such as soil aggregates, small or isolated pores, and interparticle fracture). This water retention/movement in soils is analogous to chemical sorption/transport in aquifers, which is usually a MRMT process (Zhang, Sun, et al., 2017). The FDE 4 may serve as a unified model for both processes. Notably, the introduction of chemical heterogeneity into the soil-water system leads to more variants in quantification formulas, as evidenced by the 15 chemical adsorption isotherm

models reviewed by Foo and Hameed (2010). Therefore, a unified model is needed. As demonstrated by our recent work (Zhou et al., 2021), a simplified version of the FDE 4 (see Table 1) outperforms the Langmuir and Freundlich models in capturing various adsorption isotherms of PFAS onto soils. “Multi-rate equilibrium/kinetics” may for this reason be a common feature in many soil-water systems, which cannot be reliably captured by classical models assuming a single-rate mass transfer.

The FDE 4 with a constant index captures stable equilibrium (exhibiting consistent trends and/or returning to the original status), while the FDE 4 with variable indexes accommodates transient equilibrium, reflecting changing behaviors in stages or cycles, such as hysteresis. An illustrative example is provided in Text S3 in Supporting Information S1, where the variable-index FDE 4 is the only viable model capable of capturing a non-stable wetting/drying process. Additionally, the FDE 4 generalizes Newton's law of diffusivity and Fourier's law of heat conduction, enabling the quantification of momentum and energy transport in geologic media with TSD properties (Table 1). The FDE 4 reveals transitions in momentum/energy dynamics, controlled by the truncation parameter, which were overlooked by existing models in Sun, Zhang, Wei, et al. (2018) and Zhang et al. (2021). Furthermore, it may offer insights into other kinetic processes on land surfaces involving MRMT, such as crystal growth (which is a nonlocal diffusive-controlled process whose rates are affected by various factors), rock/mineral weathering (with a spatiotemporal-scale dependent rate), and pedogenesis (where soil production and transport rates are affected by interconnected physical and bio-chemical factors) (Zhang, Sun, et al., 2017).

### Conflict of Interest

The authors declare no conflicts of interest relevant to this study.

### Data Availability Statement

The data on which this article is based are available in Siddiqui et al. (2016), Novák and Hlaváčiková (2019), and Gerolymatou et al. (2006). Our code used for this article is available from Zhang et al. (2023).

### Acknowledgments

H.G.S. was partially funded by the National Natural Science Foundation of China (Grants U2267218, 11972148, and 41931292). The results of this study do not reflect the view of this funding agency. Y. Z. was supported partially with federal funding from the Department of the Treasury under the Resources and Ecosystems Sustainability, Tourist Opportunities, and Revived Economies of the Gulf Coast States Act of 2012 (RESTORE Act). Y.Z. was also partially funded by the National Science Foundation (NSF) (Grant 2305141), United States. The statements, findings, conclusions, and recommendations are those of the author and do not necessarily reflect the views of the Department of the Treasury or ADCNR or NSF.

### References

- Baeumer, B., Benson, D. A., Meerschaert, M. M., & Wheatcraft, S. W. (2001). Subordinated advection-dispersion equation for contaminant transport. *Water Resources Research*, 37(6), 1543–1550. <https://doi.org/10.1029/2000wr900409>
- Barree, R. D., & Conway, M. W. (2005). Reply to discussion of “beyond beta factors: A complete model for Darcy, Forchheimer, and Trans-Forchheimer flow in porous media”. *Journal of Petroleum Technology*, 57(8), 73–74. <https://doi.org/10.2118/0805-0073-jpt>
- Benedikt, J., Girg, P., Kotrla, L., & Takac, P. (2018). Origin of the p-Laplacian and A. Missbach. *The Electronic Journal of Differential Equations*, 16, 1–17.
- Bolster, D., Benson, D. A., & Singha, K. (2017). Upscaling chemical reactions in multicontinuum systems: When might time fractional equations work? *Chaos, Solitons and Fractals*, 102, 414–425. <https://doi.org/10.1016/j.chaos.2017.04.028>
- Brooks, R., & Corey, A. (1964). Hydraulic properties of porous media. In *Hydrology papers*. Colorado State University.
- Cantele, M., Bal, P., Kompas, T., Hadjikakou, M., & Wintle, B. (2021). Equilibrium modeling for environmental science: Exploring the nexus of economic systems and environmental change. *Earth's Future*, 9(9), e2020EF001923. <https://doi.org/10.1029/2020ef001923>
- Chen, D., Sun, H. G., & Zhang, Y. (2013). Fractional dispersion equation for sediment suspension. *Journal of Hydrology*, 491, 13–22. <https://doi.org/10.1016/j.jhydrol.2013.03.031>
- Cvetkovic, V. (2011). The tempered one-sided stable density: A universal model for hydrological transport? *Environmental Research Letters*, 6(3), 034008. <https://doi.org/10.1088/1748-9326/6/3/034008>
- Dentz, M., Le Borgne, T., Englert, A., & Bijeljic, B. (2011). Mixing, spreading and reaction in heterogeneous media: A brief review. *Journal of Contaminant Hydrology*, 120–121, 1–17. <https://doi.org/10.1016/j.jconhyd.2010.05.002>
- Ebert, S. M., & George, L. L. (2000). *Regional ground-water flow and geochemistry in the Midwestern basins and arches aquifer system in parts of Indiana* (p. 103). US Department of the Interior, U.S. Geological Survey.
- El-Abd, A. E., & Milczarek, J. J. (2004). Neutron radiography study of water absorption in porous building materials: Anomalous diffusion analysis. *Journal of Physics D: Applied Physics*, 37(16), 2305–2313. <https://doi.org/10.1088/0022-3727/37/16/013>
- Foo, K. Y., & Hameed, B. H. (2010). Insights into the modeling of adsorption isotherm systems. *Chemical Engineering Journal*, 156(1), 2–10. <https://doi.org/10.1016/j.cej.2009.09.013>
- Forchheimer, P. (1901). Wasserbewegung durch boden. *Zeitschrift des Vereins Deutscher Ingenieure*, 45, 1781–1788.
- Gerolymatou, E., Vardoulakis, I., & Hilfer, R. (2006). Modelling infiltration by means of a nonlinear fractional diffusion model. *Journal of Physics D: Applied Physics*, 39(18), 4104–4110. <https://doi.org/10.1088/0022-3727/39/18/022>
- Giménez, D., Perfect, E., Rawls, W. J., & Pachepsky, Y. (1997). Fractal models for predicting soil hydraulic properties: A review. *Engineering Geology*, 48(3–4), 161–183. [https://doi.org/10.1016/S0013-7952\(97\)00038-0](https://doi.org/10.1016/S0013-7952(97)00038-0)
- Gu, X. T., Yu, X. N., & Zhang, G. J. (2023). Application of constant- and variable-order fractional and fractal Kelvin models to quantify uniaxial creep of frozen soil. In *prep*.
- Hassanizadeh, S. M., & Gray, W. G. (1987). High velocity flow in porous media. *Transport in Porous Medium*, 2(6), 521–531. <https://doi.org/10.1007/bf00192152>
- Horton, R. E. (1933). The role of infiltration in the hydrologic cycle. *EOS Transactions American Geophysical Union*, 14(1), 446–460.

- Iden, S. C., Diamantopoulos, E., & Durner, W. (2021). Capillary, film, and vapor flow in transient bare soil evaporation (2): Experimental identification of hydraulic conductivity in the medium to dry moisture range. *Water Resources Research*, 57(5), e2020WR028514. <https://doi.org/10.1029/2020wr028514>
- Izbash, S. V. (1935). *Construction of Dams by Dumping Stones into Flowing Water*. United States Engineer Office, Engineering Division. Translated by A. Dovjikov. Eastport, Maine. 138 Retrieved from <http://resolver.tudelft.nl/uuid:c46a945f-c0a7-4d34-bb3d-7997e52fc324>
- Jury, W. A., & Horton, R. (2004). *Soil physics* (p. 370). John Wiley and Sons, Inc.
- Knapp, A. K., Beier, C., Briske, D. D., Classen, A. T., Luo, Y., Reichstein, M., et al. (2008). Consequences of more extreme precipitation regimes for terrestrial ecosystems. *BioScience*, 58(9), 811–821. <https://doi.org/10.1641/b580908>
- Kutílek, M. (1972). Non-Darcian flow of water in soils—Laminar region: A review. *Developments in Soil Science*, 2, 327–340.
- Lewis, M. R. (1937). The rate of infiltration of water in irrigation practice. *EOS Transactions American Geophysical Union*, 18, 361–368.
- Mainardi, F. (2020). Why the Mittag-Leffler function can be considered the queen function of the fractional calculus? *Entropy*, 22(12), 1359. <https://doi.org/10.3390/e22121359>
- Meerschaert, M. M., & Tadjeran, C. (2004). Finite difference approximations for fractional advection-dispersion flow equations. *Journal of Computational and Applied Mathematics*, 172(1), 65–77. <https://doi.org/10.1016/j.cam.2004.01.033>
- Meerschaert, M. M., Zhang, Y., & Baeumer, B. (2008). Tempered anomalous diffusion in heterogeneous systems. *Geophysical Research Letters*, 35(17), L17403. <https://doi.org/10.1029/2008gl034899>
- Millington, R. J., & Quirk, J. P. (1961). Permeability of porous solids. *Transactions of the Faraday Society*, 57, 1200–1207. <https://doi.org/10.1039/tf9615701200>
- Nimmo, J. R. (2004). Porosity and pore size distribution. *Encyclopedia of Soils in the Environment*, 3(1), 295–303. <https://doi.org/10.1016/b0-12-348530-4/00404-5>
- Nimmo, J. R. (2021). The processes of preferential flow in the unsaturated zone. *Soil Science Society of America Journal*, 85(1), 1–27. <https://doi.org/10.1002/saj2.20143>
- Novák, V., & Hlaváčiková, H. (2019). Chapter 7—Soil-water retention curve. *Applied Soil Hydrology, Theory and Applications of Transport in Porous Media*, 32, 77–96. [https://doi.org/10.1007/978-3-030-01806-1\\_7](https://doi.org/10.1007/978-3-030-01806-1_7)
- Oelkers, E. H., & Schott, J. (2018). In *Thermodynamics and kinetics of water-rock interaction* (Vol. 70). Walter de Gruyter GmbH & Co KG.
- Pachepsky, Y. A., Polubesova, T. A., Hajnos, M., Sokolowska, Z., & Jozefaciuk, G. (1995). Fractal parameters of pore surface area as influenced by simulated soil degradation. *Soil Science Society of America Journal*, 59(1), 68–74. <https://doi.org/10.2136/sssaj1995.03615995005900010010x>
- Painter, S. L. (2021). On the representation of hyporheic exchange in models for reactive transport in stream and river corridors. *Frontiers in Water*, 2, 595538. <https://doi.org/10.3389/frwa.2020.595538>
- Philip, J. (1957). The theory of infiltration: 1. The infiltration equation and its solution. *Soil Science*, 83(5), 345–358. <https://doi.org/10.1097/00010694-195705000-00002>
- Rahmati, M., Latorre, B., Moret-Fernández, D., Lassabatere, L., Talebian, N., Miller, D., et al. (2022). On infiltration and infiltration characteristic times. *Water Resources Research*, 58(5), e2021WR031600. <https://doi.org/10.1029/2021wr031600>
- Richards, L. A. (1931). Capillary conduction of liquids through porous mediums. *Physics*, 1(5), 318–333. <https://doi.org/10.1063/1.1745010>
- Roche, K. R., & Dentz, M. (2022). Benthic biolayer structure controls whole-stream reactive transport. *Geophysical Research Letters*, 49(5), e2021GL096803. <https://doi.org/10.1029/2021GL096803>
- Rodríguez-Robles, C. F., Hernández-Castro, S., Hernández-Escoto, H., Cabrera-Ruiz, J., Barroso-Muñoz, F. O., & Terrazas-Rodríguez, J. E. (2019). Control analysis of batch reactive distillation column with intermittent fed. *Computer Aided Chemical Engineering*, 46, 1357–1362. <https://doi.org/10.1016/b978-0-12-818634-3.50227-7>
- Ruth, D., & Ma, H. (1992). On the derivation of the Forchheimer equation by means of the averaging theorem. *Transport in Porous Media*, 7(3), 255–264. <https://doi.org/10.1007/bf01063962>
- Samorodnitsky, G., & Taqqu, M. S. (1994). *Stable non-Gaussian random processes: Stochastic models with infinite variance*. CRC Press.
- Sanchez-Vila, X., Fernández-García, D., & Guadagnini, A. (2010). Interpretation of column experiments of transport of solutes undergoing an irreversible bimolecular reaction using a continuum approximation. *Water Resources Research*, 46(12), W12510. <https://doi.org/10.1029/2010WR009539>
- Scheidegger, A. M., & Sparks, D. L. (1996). A critical assessment of sorption-desorption mechanisms at the soil mineral/water interface. *Soil Science*, 161(12), 813–831. <https://doi.org/10.1097/00010694-199612000-00002>
- Şen, Z. (1987). Non-Darcian flow in fractured rocks with a linear flow pattern. *Journal of Hydrology*, 92(1–2), 43–57. [https://doi.org/10.1016/0022-1694\(87\)90088-6](https://doi.org/10.1016/0022-1694(87)90088-6)
- Siddiqui, F., Soliman, M. Y., House, W., & Ibragimov, A. (2016). Pre-Darcy flow revisited under experimental investigation. *Journal of Analytical Science and Technology*, 7(1), 1–9. <https://doi.org/10.1186/s40543-015-0081-2>
- Soni, J. P., Islam, N., & Basak, P. (1978). An experimental evaluation of non-Darcian flow in porous media. *Journal of Hydrology*, 38(3), 231–241. [https://doi.org/10.1016/0022-1694\(78\)90070-7](https://doi.org/10.1016/0022-1694(78)90070-7)
- Sun, H. G., Chang, A. L., Zhang, Y., & Chen, W. (2019). A review on variable-order fractional differential equations: Mathematical foundations, physical models, numerical methods and applications. *Fractional Calculus and Applied Analysis*, 22(1), 27–59. <https://doi.org/10.1515/fca-2019-0003>
- Sun, H. G., Meerschaert, M. M., Zhang, Y., Zhu, J. T., & Chen, W. (2013). A fractal Richards' equation to capture the non-Boltzmann scaling of water transport in unsaturated media. *Advances in Water Resources*, 52, 292–295. <https://doi.org/10.1016/j.advwatres.2012.11.005>
- Sun, H. G., Zhang, Y., Baleanu, D., Chen, W., & Chen, Y. Q. (2018). A new collection of real world applications of fractional calculus in science and engineering. *Communications in Nonlinear Science and Numerical Simulation*, 64, 213–231. <https://doi.org/10.1016/j.cnsns.2018.04.019>
- Sun, H. G., Zhang, Y., Wei, S., Zhu, J., & Chen, W. (2018). A space fractional constitutive equation model for non-Newtonian fluid flow. *Communications in Nonlinear Science and Numerical Simulation*, 62, 409–417. <https://doi.org/10.1016/j.cnsns.2018.02.007>
- Swartzendruber, D. (1962). Non-Darcy flow behavior in liquid-saturated porous media. *Journal of Geophysical Research*, 67(13), 5205–5213. <https://doi.org/10.1029/jz067i013p05205>
- Takhanov, D. (2011). *Forchheimer model for non-Darcy flow in porous media and fractures* (p. 31). Imperial College.
- van Genuchten, M. T. (1980). A closed-form equation for predicting the hydraulic conductivity of unsaturated soils. *Soil Science Society of America Journal*, 44(5), 892–898. <https://doi.org/10.2136/sssaj1980.03615995004400050002x>
- Verma, S., & Viswanathan, P. (2020). Bivariate functions of bounded variation: Fractal dimension and fractional integral. *Indagationes Mathematicae*, 31(2), 294–309. <https://doi.org/10.1016/j.indag.2020.01.006>
- Wang, F., Liu, Z., Cai, J., & Gao, J. (2018). A fractal model for low-velocity non-Darcy flow in tight oil reservoirs considering boundary-layer effect. *Fractals*, 26(05), 1850077. <https://doi.org/10.1142/s0218348x18500779>

- Xia, Y., Zhang, Y., Green, C. T., & Fogg, G. E. (2021). Time-fractional flow equations (t-FFEs) to upscale transient groundwater flow characterized by temporally non-Darcian flow due to medium heterogeneity. *Water Resources Research*, *57*(11), e2020WR029554. <https://doi.org/10.1029/2020wr029554>
- Zhang, Y. (2023). Adjoint models with non-Fickian reactive transport to identify pollutant sources in water. *Journal of Hazardous Materials Advances*, *12*, 100331. <https://doi.org/10.1016/j.hazadv.2023.100331>
- Zhang, Y., Baeumer, B., Chen, L., Reeves, D. M., & Sun, H. G. (2017). A fully subordinated linear flow model for hillslope subsurface stormflow. *Water Resources Research*, *53*(4), 3491–3504. <https://doi.org/10.1002/2016wr020192>
- Zhang, Y., Benson, D. A., & Baeumer, B. (2008). Moment analysis for spatiotemporal fractional dispersion. *Water Resources Research*, *44*(4), W04424. <https://doi.org/10.1029/2007wr006291>
- Zhang, Y., Meerschaert, M. M., Baeumer, B., & LaBolle, L. M. (2015). Modeling mixed retention and early arrivals in multidimensional heterogeneous media using an explicit Lagrangian scheme. *Water Resources Research*, *51*(8), 6311–6337. <https://doi.org/10.1002/2015wr016902>
- Zhang, Y., Sun, H. G., Stowell, H. H., Zayernouri, M., & Hansen, S. E. (2017). A review of applications of fractional calculus in Earth system dynamics. *Chaos, Solitons & Fractals*, *102*, 29–46. <https://doi.org/10.1016/j.chaos.2017.03.051>
- Zhang, Y., van Genuchten, M. T., Zhou, D. B., Zhang, G. J., & Sun, H. G. (2023). A unified phenomenological model captures water equilibrium and kinetic processes in soil: Codes. December 30, 2023 Release (version 1.0) [Software]. *Zenodo*. <https://doi.org/10.5281/zenodo.10445660>
- Zhang, Y., Yu, X., Fleckenstein, J. H., Sun, H. G., Lu, C., Yin, M., et al. (2021). Upscaling heat flow in porous media with periodic surface temperature fluctuation using a one-dimensional subordinated heat transfer equation. *Water Resources Research*, *57*(7), e2020WR027266. <https://doi.org/10.1029/2020wr027266>
- Zhao, Y. (2020). Calculating the pore fractal dimension of porous media by using pore size distribution. *Data Processing Techniques and Applications for Cyber-Physical Systems (DPTA 2019)*, 785–792. [https://doi.org/10.1007/978-981-15-1468-5\\_92](https://doi.org/10.1007/978-981-15-1468-5_92)
- Zhou, D., Brusseau, M. L., Zhang, Y., Li, S., Wei, W., Sun, H. G., & Zheng, C. M. (2021). Simulating PFAS adsorption kinetics, adsorption isotherms, and nonideal transport in saturated soil with tempered one-sided stable density (TOSD) based models. *Journal of Hazardous Materials*, *411*, 125169. <https://doi.org/10.1016/j.jhazmat.2021.125169>